Title
Reactivity of Uranium and Ferrous Iron with Natural Iron Oxyhydroxides

Journal
Environmental Science and Technology, 49(17)

ISSN
0013-936X

Authors
Stewart, Brandy D
Cismasu, A Cristina
Williams, Kenneth H
et al.

Publication Date
2015-09-01

DOI
10.1021/acs.est.5b02645

Peer reviewed

Reactivity of Uranium and Ferrous Iron with Natural Iron Oxyhydroxides

Brandy D. Stewart[†], A. Cristina Cismasu[‡], Kenneth H. Williams[‡], Brent M. Peyton[†], and Peter S. Nico[*‡]

[†] Chemical and Biological Engineering, Montana State University, Bozeman, Montana 59717, United States

[‡] Lawrence Berkeley National Laboratory, Earth Sciences Division, Berkeley, California 94720, United States

*Phone: 510-486-7118; e-mail: psnico@lbl.gov.

DOI: 10.1021/acs.est.5b02645

Publication Date (Web): July 30, 2015

Abstract

Determining key reaction pathways involving uranium and iron oxyhydroxides under oxic and anoxic conditions is essential for understanding uranium mobility as well as other iron oxyhydroxide mediated processes, particularly near redox boundaries where redox conditions change rapidly in time and space. Here we examine the reactivity of a ferrihydrite-rich sediment from a surface seep adjacent to a redox boundary at the Rifle, Colorado field site. Iron(II)–sediment incubation experiments indicate that the natural ferrihydrite fraction of the sediment is not susceptible to reductive transformation under conditions that trigger significant mineralogical transformations of synthetic ferrihydrite. No measurable Fe(II)-promoted transformation was observed when the Rifle sediment was exposed to 30 mM Fe(II) for up to 2 weeks. Incubation of the Rifle sediment with 3 mM Fe(II) and 0.2 mM U(VI) for 15 days shows no measurable incorporation of U(VI) into the mineral structure or reduction of U(VI) to U(IV). Results indicate a significantly decreased reactivity of naturally occurring Fe oxyhydroxides as compared to synthetic minerals, likely due to the association of impurities (e.g., Si, organic matter), with implications for the mobility and bioavailability of uranium and other associated species in field environments.

Introduction

Mining and nuclear enrichment activities throughout the last century have created a legacy of uranium and cocontaminants in the environment. Within the U.S. alone uranium has been located in over 3000 *inactive* waste disposal areas within the Department of Energy (DOE) Complex,(1) in addition to more than 20 *inactive* uranium mill tailing sites in 10 states.(2) In many cases, uranium, a contaminant of concern due to its toxic effects and radioactivity, has migrated from waste disposal sites to surrounding soils, sediments, and waters where its fate is often controlled by redox and sorption processes, and in particular the proportion of U(VI) to U(IV).(3) Understanding the stability and mobility of these U-bearing materials is critical to the DOE remediation effort. In recent years uranium transformation and mobility has been studied extensively at the DOE Old Rifle former mill site near Rifle, CO where uranium was processed from 1942 to 1958. Despite the removal of mill tailings and surface waste between 1992 and 1996, uranium contamination in the underlying sediments and aquifer persists today.(4)

Redox fluctuations can promote the dissolution of iron bearing minerals (including iron oxides) and the precipitation of fresh Fe(III) precipitates, influencing the surrounding biogeochemistry. Thompson et al. report that iron oxide crystallinity generally increases during redox fluctuations(5)and that newly formed oxides may include impurities, such as metals, oxyanions and organic acids.(6) Additionally, iron oxidation under low dissolved oxygen conditions (i.e., in redox transition areas) can promote formation of both organic Fe(III) complexes and disordered, impure ferrihydrite-organic matter coprecipitates.(6-8) The reactivity of these fresh precipitates is particularly relevant for the sorption and coprecipitation of other metals and organic matter, and their reactivity and stability in the environment may influence the ultimate fate of these species.

Fe oxyhydroxides are strong sorbents of uranium due to their high reactivity,(9) their high surface area (<50m^2/g) and prevalence in natural systems. Uranium and Fe have been found concomitantly in environmental settings over a vast range of temporal scales. Some studies have observed the association of U and Fe on geologic time scales on the order of millions of years.(10)Uranium has also been found in association with Fe and phosphate mineral phases at the DOE Oak Ridge, TN nuclear reservation,(11) in close association with sediments naturally elevated in organic matter(12) and in mine wastes(13) where associations have formed within the last ~75 years. Both U adsorption to oxide surfaces followed by incorporation, as well as U and Fe oxyhydroxide coprecipitation have been postulated as potential explanations for U–Fe association.(14) Accordingly in recent years, several studies have observed U incorporation into synthetic Fe oxides under a variety of experimental conditions including during Fe(II) promoted reductive transformation(15) of Fe(III) oxyhydroxides. In several of these studies U(VI) was removed from solution, remained in an oxidized form and was found both adsorbed on and incorporated into the structure of newly formed goethite and magnetite.

Here we provide evidence for the persistence of a natural ferrihydrite-rich material adjacent to the Old Rifle site in the presence of Fe(II) and U(VI) in a redox boundary region. Owing to the complexity of natural samples, we examine the compound impact of multiple impurities (trace metals and organic matter, which may be present within the structure or on the surface of the Fe(III) mineral) on Fe(II)-promoted transformation, as well as the potential for

uranium uptake during iron oxyhydroxide transformations induced by Fe(II). Additionally we evaluate the potential of the natural sediment as an adsorbent for U(VI) as compared to synthetic ferrihydrite.

Materials and Methods

Chemical Extractions

Field samples were collected aseptically and placed in sterile plastic tubes before being placed on dry ice and expedited to Montana State University where they were stored at −80 °C until the time of experiments. Immediately prior to experiments sediments were dried, pieces of debris (primarly rock) were removed, and samples were homogenized by gently crushing with a mortar and pestle. The unreacted sediment was silty clay, very fine, and bright reddish-brown in color.

Chemical extractions were carried out to estimate the total iron bound in Fe oxyhydroxides, the amount of Fe bound in poorly crystalline oxyhydroxides, the amount of inorganic impurities (e.g., Si, Al, Mn, etc.), and the amount of organic carbon released. The modified inorganic dithionite extraction developed by Wagai and Mayer(16) was used to determine total reactive Fe bound in Fe oxides; this version of the citrate-dithionite extraction was chosen since it does not include citrate, and thus allowed us to quantify the organic carbon content of the extract. The extraction procedure consisted of reacting 100 mg of sediment in 30 mL of a 0.05 M sodium dithionite solution (pH 4.4) for 16 h at room temperature on a rotational shaker. Subsequent to the reaction period, solids were separated by centrifugation (40 min at 35 000*g*) and resuspended in 30 mL of a 0.5 M HCl solution at room temperature for an hour to dissolve any Fe that precipitated as acid-volatile sulfides; this second extract was also collected after centrifugation (40 min at 35 000*g*).

An additional hydroxylamine hydrochloride extraction(17) was used to estimate the amount of Fe bound in poorly crystalline Fe oxyhydroxides, the amount of trace metal(loids) and organic carbon released. This procedure consisted of reacting 100 mg of sediment in 25 mL 0.25 M hydroxylamine hydrochloride +0.25 M HCl solution (pH 0.8), for 1 h in a water bath at a temperature of 50 °C under moderate shaking. These suspensions were filtered using a 0.45 μm filter prior to ICP-MS analysis. The composition of each extract was obtained using a PerkinElmer SCIEX Elan DRC II inductively coupled plasma mass spectrometer. Total organic and inorganic carbon contents in the unreacted sediment and in the hydroxylamine hydrochloride and dithionite extracts were measured using a Shimadzu TOC-VCSH high sensitivity inorganic/organic carbon analyzer, which is also equipped with a SSM-5000A module for solid sample analysis. Finally, a total digestion was performed using ALS Minerals Methods ME-MS81/ICP06 where samples were fused at 1000 °C in lithium metaborate/lithium tetraborate flux followed by dissolution in 4% nitric acid/2% hydrochloric acid and analysis by ICP-AES/MS.

Incubation Experiments

Three sets of batch experiments were conducted to examine the reactivity of the unreacted sediment toward Fe(II) and U. The first of these examined the reactivity of the sediment toward Fe(II). Systems contained 0.5 g unreacted Rifle sediment, 50 mL PIPES buffered distilled–deionized (DDI) water (10 mM PIPES, pH 7) and varying

concentrations of ferrous sulfate ($FeSO_4$) (3, 10, or 30 mM). Solutions were made anoxic (<0.02 mg/L) by boiling and cooling under a stream of N_2 gas and systems were assembled under anoxic conditions in a glovebag (Coy Laboratory Products) with a N_2 (90%):H_2 (5%):CO_2(5%) atmosphere. Experiments were deconstructed and aqueous Fe(II) concentrations measured at the end point of each experiment (2, 8.5, and 14 weeks) where ca. 1.5, 7, and 18 mM Fe(II) remained for 3, 10, 30 mM starting concentrations respectively (irrespective of incubation time).

A second experiment examined the interaction of the sediment and U(VI) (adsorption). A parallel set of experiments were run with synthetic ferrihydrite and U(VI) for comparison to the Rifle sediment. Ferrihydrite was prepared according to the method described by Brooks et al.(18) A solution of ferric chloride was rapidly titrated with sodium hydroxide over a period of approximately 10 min until a pH of 7 was reached. Chloride and sodium were then removed from the ferrihydrite with sequential rinses. Ferrihydrite was then dried and purity of product was confirmed using XRD. Adsorption batch systems contained 0.2 g of unreacted sediment or ferrihydrite, and 100 mL PIPES buffered distilled–deionized (DDI) water (10 mM, pH 7) with the following components: 1 mM $CaCl_2$, 3.8 mM $KHCO_3$, and varying concentrations of uranyl acetate ranging from 0 to 0.15 mM. pH and chemistry remained constant throughout the experiment.

The final batch experiment studied the interaction of the sediment with U(VI) and Fe(II) concurrently. Experiments contained unreacted sediment, PIPES buffered distilled–deionized (DDI) water (10 mM, pH 7), 3 mM $CaCl_2$, 3 or 10 mM $FeSO_4$, and 0.2 mM uranyl acetate. Solutions were made anoxic as described above. All experiments were shaken at 85 rpm at 25 °C outside of the glovebag and were conducted in triplicate. All U(VI) concentrations were measured on a kinetic phosphorescence analyzer (KPA) instrument (Columbus Instruments). Samples were vacuum filtered, rinsed with DDI, dried, and sealed inside Kapton tape prior to XRD and XAS analysis.

XRD Analysis

Micro X-ray diffraction (μXRD) data for the unreacted Rifle sediment and for sediment reacted with 3, 10, and 30 mM Fe(II) for 8.5 weeks were collected at the Stanford Synchrotron Radiation Lightsource (SSRL) beamline 11–3 at an energy of 12.7 keV, which corresponds to a wavelength of 0.9762 Å, using a beam spot size of 0.1 mm. A thin sediment powder film was sandwiched in Kapton tape for all measurements. Data were collected on a MAR 3450 detector at a sample–detector distance of ∼150 mm. Five frames, each exposed for 250 s were collected for each sample over different sample areas; data were also collected on a blank sample (Kapton tape), which allowed for subtraction of scatter resulting primarily from the sample mount (background). Calibration of the sample to detector distance was done using a lanthanum hexaboride standard (LaB_6). Raw data were integrated using the software Fit2D(19) and the background (Kapton) subtraction was done using the software XRD-BS.

X-ray Absorption Spectroscopy

Fe K-edge X-ray absorption spectroscopy data for the unreacted and Fe(II)-reacted samples (3, 10, and 30 mM Fe(II) for 2 weeks; 3 mM Fe(II) for 8.5 weeks; 3 mM Fe(II) for 14 weeks) were collected at room temperature at the Stanford Synchrotron Radiation Lightsource, beamline 11–2, using a Stern-Heald (Lytle) detector and a Si 220 double-crystal monochromator in a phi = 0 orientation (additional details found in Supporting Information).

Data extraction, processing, least-squares fits and principal component analyses were done using the SixPack software package.(20) k^3-weighted EXAFS (k_{max} = 13 Å^{-1}) were used for principal component analysis (PCA) and linear combination fits (LCF) to determine the number, type and proportion of the predominant Fe phases as a function of reaction with Fe(II). PCA was carried out initially to constrain the minimum number of components needed to describe the data set by using all six Fe EXAFS spectra of the unreacted and Fe(II)-reacted samples. Two major components were found to describe the data set, according to variance values of 0.7 and 0.1 for the first two components, which indicate that one major and one secondary phase explain up to 80% of variance within the series of spectra. Target transformations were used subsequently to identify mineral phases that constitute probable components in the experimental data set. Ferrihydrite yielded a good fit according to target transformations; smectite also appeared suitable, although a poorer fit was obtained. Target transforms were also carried out against additional reference compounds (goethite, hematite, magnetite, hydroxycarbonate green rust, siderite, pyroxene, hornblende, biotite) but did not provide satisfactory fits, indicating that these phases are likely not abundant in the Rifle sediment.

LCFs were carried out using the Fe-bearing phases identified by PCA and XRD, that is, ferrihydrite and smectite, and fit attempts using other reference spectra were not successful. For all LCFs, component sums were set to 1, and similar results were obtained without this constraint. Data were allowed to shift in energy during fitting, with maximum obtained shifts of 0.05 eV.

U L_{III}-edge X-ray absorption spectroscopy data for the unreacted sediment and U(VI)–Fe(II) reacted sediments were also collected at Stanford Synchrotron Radiation Lightsource, beamline 11–2 (double crystal Si220 monochromator using a 30-element germanium detector). Energy calibration was monitored using a Y foil. Spectra for a sample of U(VI) adsorbed onto synthetic ferrihydrite were collected under similar experimental conditions for comparison.

Results and Discussion

Field Sampling Collection

Samples were collected from a hillside seep located directly to the north and upgradient from the U.S Department of Energy Rifle, CO field site (photograph of field site in Supporting Information). Field measurements showed nondetectable concentrations of O_2 in the water at the head of the seep closest to the hillside. This is consistent with low groundwater O_2 concentrations present within an alluvial aquifer directly downgradient of the seep.(21) Within ~1m of the seep origin dissolved O_2 increased to ca. 10.7 mg/L, while pH remained constant at 6.9. The detected change from reduced to oxic conditions were supported by dramatic decreases in the concentration of both Mn and Fe from ca. 790 and ca. 3760 ug/L at the head of the seep to 12 and <10 ug/L, respectively, ~ 1m downgradient indicating oxidative precipitation of these two redox sensitive elements. This was consistent with the appearance of a red, iron-rich precipitate as the water flowed at the surface and became oxygenated. Beyond spring and seep discharge localities encountered globally, the conditions described here are equally characteristic of redox boundaries encountered under a diversity of environmental conditions. These include capillary fringe sediments exposed to variably saturated conditions accompanying fluctuations in groundwater, anoxic aquifer sediments seasonally infiltrated by oxygenated meltwater and precipitation, and hyporheic interfaces between anoxic

groundwater and adjoining surface waters. Each of the aforementioned conditions exists at the adjoining Rifle field site, and as such, the results reported here for redox boundaries at circumneutral conditions and the resulting precipitates are deemed representative of the types of materials that could form at such boundaries.

Composition of the Fe-Rich Sediment Fraction

Two chemical extractions were used to evaluate the composition of the Fe oxyhydroxides in the unreacted sediment. The composition of the poorly crystalline, hydroxylamine-hydrochloride extractable component of the sediment is given in Table 1 along with results of the sodium dithionite extraction, which accounts for total reactive iron. Extractions were completed in triplicate and results shown are averages. The results of the two extractions and a total digestion are comparable in terms of Fe content, 43, 44, 42 mg/g respectively, suggesting that the vast majority of the Fe is associated with poorly crystalline phases. Significant calcium (49 mg Ca/g sediment), as well as Mg and Si (up to 4 and 5 mg/g sediment, respectively), Al and Mn (up to 0.6 and 1 mg/g sediment) were also extracted. In both extractions, the Al:Fe and Mn:Fe molar ratios are ~0.02, whereas the Si:Fe ratio is 10 times larger, ~0.2. Vanadium and strontium are the most abundant trace impurities, at concentrations of up to 0.13 and 0.46 mg/g, respectively. The total organic carbon (TOC) content in the dry sediment is ~3.8%, and total inorganic C (TIC) is ~1.9%. Organic C was also measured in the hydroxylamine and the dithionite extracts, and values of 15.3 and 24.8 mg C/g were obtained, respectively, which correspond to molar C:Fe ratios of ~1.5.

Table 1. (a) Composition of the Hydroxylamine Hydrochloride Extract (Hydroxylamine HCl), Used to Approximate Fe Bound in Poorly Crystalline Phases in the Unreacted Sediment, The Sodium Dithionite Extract (Na Dithionite), Which Estimates Total Reactive Fe, and the Total Digestion Extract. (b) Total Inorganic Carbon (TIC) and Total Organic Carbon (TOC) Determined in the Bulk Sediment

	hydroxylamine HCl (pH 0.8)		Na dithionite (pH 4.4)		
(a)	avg	stdev	avg	stdev	total digestion[9]
Si	4.3	0.1	5.0	0.1	102
Al	0.56	0.01	0.62	0.01	22
Fe	43	2	44	1	42

	hydroxylamine HCl (pH 0.8)		Na dithionite (pH 4.4)		
(a)	**avg**	**stdev**	**avg**	**stdev**	**total digestion[q]**
Mn	0.93	0.05	1.0	0.2	2.7
Mg	4.3	0.3	3.51	0.09	9.0
Ca	49	5.3	49	2	165
K	0.14	0.01	0.4	0.1	4.3
V	0.123	0.004	0.129	0.005	0.148
Se	0.0065	0.0003	0.008	0.001	0.016
Ni	0.008	0.003	0.0065	0.0002	0.008
Co	0.0055	0.0002	0.0058	0.0005	0.015

	hydroxylamine HCl (pH 0.8)		Na dithionite (pH 4.4)		
(a)	**avg**	**stdev**	**avg**	**stdev**	**total digestion[a]**
Cu	0.009	0.001	0.0122	0.0002	0.012
Zn	0.0358	0.0002	0.19	0.01	0.047
As	0.062	0.002	0.0688	0.002	0.042
Sr	0.460	0.02	0.46	0.02	1.01
U	0.0057	0.0003	0.0041	0.0001	0.009
C_{org}	15.27		24.78		

(b)		
TOC[b]	%	3.8
TIC[b]	%	1.9

[a] mg/g sediment.

[b] Total organic and inorganic C in sediment measured on solid phase.
[c] ALS Minerals Methods ME-MS81/ICP06: sample fused at 1000 °C in lithium metaborate/lithium tetraborate flux followed by dissolution in 4% nitric acid/2% hydrochloric acid and analysis by ICP-AES/MS.

Selective dissolution using ammonium oxalate or hydroxylamine hydrochloride solutions is generally used as an indication for the occurrence of ferrihydrite-like Fe oxyhydroxides in complex natural samples,(22) and coextracted impurities e.g., Al, Si, P, As generally assumed to be closely associated with these precipitates.(23) Organic carbon association with natural Fe oxyhydroxides is also common, with C:Fe ratios of 0.3 for ferrihydrite-rich flocs in groundwater at the Rifle site,(24) and higher ratios, between 0.2 and 12 for soils,(16, 25) between ∼2 and 5 for lacustrine Fe oxyhydroxides,(26) and between 0.2 and 10 for freshwater, estuarine and marine sediments.(27)Although it is difficult to confirm the exact origin of the (in)organic species, and crystalline phases or additional poorly crystalline phases may partially or completely dissolve during chemical extraction, it is also well-known that poorly crystalline Fe oxyhydroxides are highly reactive toward various ions and organic molecules. For the purpose of this work, we assume that a large fraction of the major organic and inorganic impurities released by the hydroxylamine hydrochloride extraction (e.g., organic matter, Si) are associated with ferrihydrite in the Rifle sediment, either by means of incorporation or adsorption/surface precipitation.

The association of inorganic impurities and natural organic matter with natural ferrihydrite is frequent, has been observed in a variety of environments,(5, 22b) and is known to impact ferrihydrite properties, such as particle size, crystallinity, aggregation, particle surface composition, and overall chemical reactivity. There is evidence indicating that the presence of inorganic impurities, e.g. Al,(28) phosphate(29) and silica,(30) and coprecipitation with organic compounds(31) can retard Fe(II)-induced transformations to more crystalline Fe oxyhydroxides.

X-ray Diffraction of the Sediment

X-ray diffraction data for the unreacted and reacted Rifle sediment (Figure 1A) indicate the presence of abundant crystalline phases, although none that are dominated by Fe. We identified several minerals, namely quartz, feldspar, Illite, as well as calcite. The background of all diffraction patterns shows the presence of a diffuse scattering component, defined by broad features centered at approximately 22 and 38 degrees, which correspond to the ferrihydrite *d*-spacings at ∼2.5 and ∼1.5 Å, respectively (Figure 1B). Although weak, these features are present consistently in all four samples, even in the 3, 10, and 30 mM Fe(II)-reacted samples (only data for the unreacted sediment and the 30 mM Fe(II)-reacted sample are shown in Figure 1B).

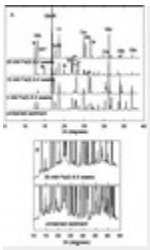

Figure 1. (A) XRD data (λ = 0.9762 Å) for unreacted sediment and for sediment that has been reacted with 3, 10, and 30 mM Fe(II) for 8.5 weeks; crystalline phases identified are quartz (Qtz), calcite (Ca), feldspar (Fsp) and Illite (Ilt); goethite (Gt) may be present in the sample reacted with 30 mM Fe(II). (B) Diffuse scattering component for selected samples (unreacted sediment and 30 mM Fe(II) reacted sediment). The broad features centered at ∼22 and 38 degrees are assigned to ferrihydrite.

Overall, the sample series appears rather heterogeneous in terms of crystalline mineral phases; minerals such as Illite, for example, were identified only in the unreacted sample and in the 10 mM Fe(II) reacted sample. This may be due to both sample complexity and heterogeneity, combined with the limitations of μXRD measurements using a 0.1 mm X-ray beam. In addition, we did not observe the formation of more crystalline Fe oxyhydroxide minerals upon reaction with Fe(II). We were particularly interested in identifying reductive transformation products along the sample series, namely an increase in goethite, lepidocrocite, magnetite, etc. However, ferrihydrite predominates throughout the series of XRD spectra as the major Fe oxyhydroxide phase, and we found only one minor indication for the presence of goethite in the sample reacted with 30 mM Fe(II) for 8.5 weeks (although XRD cannot definitely rule out other nanoparticulate or amorphous Fe phases). This weak feature corresponds to the strongest goethite reflection, which occurs at ~13.4 degrees. No other peaks typical for goethite could be identified in this diffractogram possibly due to a very low goethite content, and although it is possible for goethite to form as a result of the interaction of ferrihydrite with Fe(II), we cannot be absolutely certain of its presence based only on one Bragg peak.

Fe K-Edge XANES and EXAFS

Fe K-edge XANES spectra (Figure 2) for the unreacted sediment and Fe(II)-reacted solids (3, 10, and 30 mM Fe(II) for 2 weeks; 3 mM Fe for 8.5 weeks; 3 mM Fe(II) for 14 weeks) appear identical despite significant differences in the amount of Fe(II) reacted with the sediment (3 to 30 mM Fe(II)) and increasing reaction times (from 2 to 14 weeks). The spectra shown in Figure 2 have equivalent edge and pre-edge profiles, that is, there are no shoulders, broadening, or shifts in energy in the edge or pre-edge regions for the Fe(II)-reacted samples.

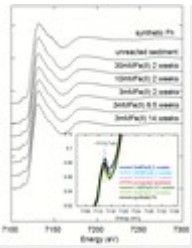

Figure 2. Fe K-edge XANES for unreacted and Fe(II)-reacted sediment for 2, 8.5, and 14 weeks; inset illustrates pre-edge feature situated at an energy of ~7113.7 eV; the Fe K-edge XANES for synthetic ferrihydrite is shown for comparison.

The position and intensity of the pre-edge feature is particularly sensitive to Fe oxidation state and coordination, (32) and has been used to evaluate the chemistry of Fe in several environments, in sediments, groundwater and surface precipitates, soils, weathering products and glasses. Pre-edges are related to 1s-3d and 1s-4p metal electronic transitions, and shift to higher energy with increasing oxidation state. For Fe(II)-bearing phases, the centroid position of the pre-edge feature is situated at approximately 7112.1 eV, whereas its position shifts toward ~7113.7 eV for Fe(III). The pre-edge also exhibits variable and distinctive intensities that are related to coordination environment. For example, in the case of Fe(III) compounds, the highest pre-edge intensity has been linked to the presence of noncentrosymmetric geometry, or tetrahedral Fe^{3+} coordination. The position of the pre-edge feature for the unreacted and Fe(II)-reacted samples of this study is at an energy of ~7113.7 eV, similar to synthetic ferrihydrite (see inset of Figure 2), and iron is expected to be primarily in ferric form. Furthermore, no systematic

variations in pre-edge shape or intensity occur along the sample series, which suggests that the Fe coordination environment is not affected at these conditions as a result of reaction with Fe(II).

Fe K-edge EXAFS also indicate that no systematic changes occur in the EXAFS oscillation intensities or positions as a result of the amount of Fe(II) reacted with the sediment (3 to 30 mM), or with increasing reaction time. In order to evaluate in a more quantitative manner any changes in mineralogy as a result of this reaction, principal component analyses (PCA) and linear combination fits (LCF) were carried out on the Fe K-edge EXAFS spectra (Figure 3). PCA were carried out to constrain the minimum number of components, and to identify probable components needed to describe the data set. PCA results show that two principal components reproduce the experimental data set reasonably well (Figure 3A). Target transformations were used to identify possible model compounds from a set of reference spectra, which included ferrihydrite, smectite, goethite, hematite, magnetite, green rust, siderite, biotite, pyroxene, and amphibole. Two model compounds were found to yield satisfactory fits according to target transformations, namely ferrihydrite and to a lesser extent, smectite (see Figure 3A for target transform results). Ideally, an Fe-bearing Illite standard would have been suitable for these analyses, since this phase was identified by means of XRD in the sediment. Here we use a ferrous smectite as a model compound, which approximates well the Fe K-edge EXAFS spectrum of Fe-bearing Illite, when compared to literature results. (33)

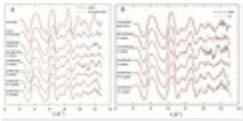

Figure 3. (A) Experimental and reconstructed Fe K-edge EXAFS for the unreacted and reacted sediment, and for reference smectite and ferrihydrite spectra. The fits obtained from spectrum reconstructions indicate that the Fe EXAFS of the Rifle sediment series can be described reasonably well by using only two principal components. Target transformations indicate a good fit to ferrihydrite and smectite, and these were identified as probable phases contained in the unreacted and Fe(II)-reacted Rifle sediment. (B) Fe K-edge EXAFS and linear combination fit results for unreacted and Fe(II)-reacted sediment, using ferrihydrite and smectite as spectral components. LCF component proportions are given in Table 2.

LCFs were carried out on the Fe EXAFS and yielded best fits for all samples when using ferrihydrite and smectite as Fe spectral components (Figure 3B). The proportion of ferrihydrite obtained by LCF varies from 74 to 94% of the Fe EXAFS signal for the series of experimental spectra, and the proportion of ferrihydrite is not correlated with Fe(II) amount or reaction time (Table 2). In the case of the Fe(II)-reacted samples, fits were carried out initially using only ferrihydrite and smectite, but additional Fe(II)/Fe(III) oxyhydroxide components, for example, goethite, lepidocrocite, hematite, carbonate/sulfate green rust, siderite and magnetite were included in the fit subsequently to test any possible improvement in the fit quality. No significant improvement was obtained (changes in reduced chi sq. < 0.04) by means of this procedure.

Table 2. Fe K-Edge EXAFS Linear Combination Fit Results for Unreacted and Fe(II)-Reacted Sediments

LCF components	unreacted sediment	3 mMFe(II) 2 weeks	10 mMFe(II) 2 weeks	30 mMFe(II) 2 weeks	3 mMFe(II) 8.5 weeks	3 mMFe(II) 14 weeks
ferrihydrite	74%	82%	77%	94%	79%	77%
smectite	26%	19%	23%	6%	21%	23%
Red. Chi-Sq:	*0.25*	*0.18*	*0.42*	*0.28*	*0.38*	*0.41*

Some visible misfits occur at *k* values between 9 and 13 $Å^{-1}$ for all samples except for the unreacted sample and 3 mM Fe(II) 8.5 weeks (Figure 3). These misfits are not systematic, i.e. there are no correlations with Fe(II) reaction amount/time. Overall, PCA results combined with linear combination fits and the qualitative analysis of the Fe XANES pre-edge, and the chemical extraction results suggest that ferrihydrite is the major Fe(III)-bearing phase in the Rifle sediment, and that its reaction with 3 mM Fe(II) for up to 14 weeks and 30 mM Fe(II) for up to 2 weeks did not promote reductive transformation to more crystalline Fe oxyhydroxides. However, XRD results hint that small amounts of goethite may have formed after 8.5 weeks of exposure to 30 mM Fe(II).

The ferrihydrite fraction of the unreacted sediment contains appreciable levels of cations including Al, Si, Mn, and organic matter (Table 1). The impact of substitution and/or adsorption, as well as OM association on Fe(II)-promoted transformation of ferrihydrite to more crystalline phases including goethite, lepidocrocite, and magnetite has been evaluated in several studies.(28) Masue et al.(28c) found that Al substituted into the structure of ferrihydrite, along with As adsorbed on the surface completely inhibited transformation to other phases with Fe(II) levels of 1.7 mM, whereas Hansel(28a) observed that Al adsorbed to the surface of ferrihydrite had a greater impact than substitution on impeding transformation to other phases. Additional studies have shown that phosphate(29) as well as silica(31) also impact variably transformation rates and products. Finally, the reductive transformation of synthetic ferrihydrite–humic acid coprecipitates also appeared to be affected by the amount of organic C, with slower reduction rates at C/Fe ratios ≤0.8 and higher rates at C/Fe ratios ≥1.8.(33) We suggest that the amount and types of impurities contained in the Rifle ferrihydrite (Table 1) play a central role in the observed inhibition, or delay of Fe(II)-mediated reductive transformation.

Uranium(VI) Adsorption onto Sediment and Ferrihydrite

Figure 4 compares the U(VI) adsorptive capacity of the unreacted Rifle sediment with synthetic ferrihydrite. The results indicate that on a per Fe basis the synthetic ferrihydrite has a significantly larger capacity to adsorb U(VI) than the unreacted Rifle sediment (Figure 4). This may be attributed to a combination of higher reactive Fe surface

area as compared to the sediment, and/or a lower affinity of surface sites on the sediment toward U(VI). When results are normalized for both Fe content and surface area there is still significantly more (>10x) U(VI) associated with the ferrihydrite than with the Rifle sediment (i.e., per mol Fe and per m^2), suggesting that the primary reason for differences in adsorption behavior is a discrepancy in site availability for U(VI). In this case, we hypothesize that a portion of surface sites on the natural sediment are occupied by other ions (e.g., Si), or that particle surfaces exhibit surface precipitates/polymers (e.g., Si polymers) and/or organic coatings. Several studies on synthetic and natural Si-bearing ferrihydrite indicate that Si is likely not incorporated in the ferrihydrite structure, but rather resides at particle surfaces,(34) and this can have an impact on metal(loid) adsorption capacity and surface speciation. Additionally, the presence of organic molecules at mineral surfaces has also been shown to significantly impact U(VI) adsorption and desorption reactions;(35) a potential explanation for the observation of decreased uranium adsorption on the Rifle sediment.

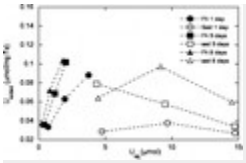

Figure 4. Uranium adsorption curves comparing synthetic ferrihydrite and unreacted sediment on a per mg Fe basis.

Sediment Interaction with U(VI) and Fe(II)

Results from experiments in which the Rifle sediment was incubated with both U(VI) and Fe(II) concurrently suggest that no major mineralogical transformation occurred during the course of the experiment. Sediments did not appear to change dramatically in color as we observed in similar previous studies with synthetic ferrihydrite where an appreciable fraction of ferrihydrite transformed to magnetite and goethite with U incorporated into the mineral matrix.(15b, 36) Figure 5 illustrates that within the estimated <5–10% error of XANES analysis,(37) the oxidation state and local coordination chemistry of Fe and U are comparable to Fe(III) in ferrihydrite (in the case of Fe) and to U(VI) adsorbed on the surface of synthetic ferrihydrite in the case of U (the minor differences between the Fe spectra in Figure 5 are consistent with classic “overabsorption” or “self-absorption” distortions(38)). These results further support an increased stabilization of the ferrihydrite in the Rifle sediment, and also indicate that U binds preferentially to Fe reactive sites, in spite of their lower availability at the ferrihydrite surface (Figure 4).

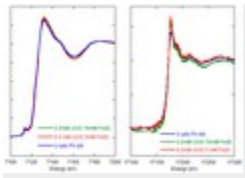

Figure 5. Iron K-edge (A) and uranium L-edge (B) XANES results for unreacted sediment reacted with 0.2 mM U(VI) and 3 or 10 mM Fe(II) compared to synthetic ferrihydrite (A) and U adsorbed on the surface of ferrihydrite (B); local coordination environment of U and Fe in reacted sediment is similar to standards in both cases.

These results suggest that appreciable levels of Fe(II) are not incorporated into the sediment, nor is there significant Fe(II) associated with the solid surface. This is consistent with results from the Fe(II) incubation experiments (described above) where no transformation of the Rifle sediment to more crystalline Fe(III)/Fe(II) minerals was

detected. This result is perhaps unsurprising given that adsorption of Fe(II) to the surface of ferrihydrite (or similar material) is a required step in Fe(II)- promoted mineral transformation,(39) a precursor for U incorporation into the solid.(15b, 15d)Additionally, Massey et al. recently observed that Al substituted into synthetic ferrihydrite at levels as low as 1 mol % decreased incorporation of U into Fe mineral structure during Fe(II) promoted transformation by ∼20% (Massey personal communication).

Implications

Comparing the reactivity of synthetic materials to field materials and elucidating the impact of mineral impurities, both within mineral structure and associated with surfaces, on potential transformation of poorly crystalline Fe(III) hydroxides is critical to accurately predicting both iron mineral transformation pathways and the fate of metals and organic matter associated with these minerals. Our results show dramatic differences in the rates and extent of transformation of Fe minerals and associated U with natural field materials as compared to those reported for laboratory systems. The materials used here are likely to be representative of a large class of naturally occurring ferrihydrite-like materials that form from complex natural waters at abrupt redox boundaries. Therefore, the decreased reactivity of the materials examined herein should be considered when predicting the fate of iron minerals and their associated species, such as U and organic matter. Dissolution of these minerals could result in the release of contaminant metals and oxyanions including U, while stability or persistence of these impure or substituted oxides could foreseeably result in attenuation of metal and metalloid pollutants through continued association with a more recalcitrant solid phase. While Fe(III) associated with these coprecipitated oxyhydroxides may be bioavailable for respiration by metal reducing microorganisms, resulting in elevated Fe(II) levels, the transformation of these materials is expected to be delayed (as compared to predictions based on synthetic ferrihydrite) as a result of exposure to Fe(II). Results shown here could help to explain the observed uranium concentrations present in these solids that appears to be both oxidized and stable (immobile) and suggests a potential means for natural uranium attenuation that is stable under both oxic and anoxic conditions.

Acknowledgment

We thank Aaron Slowey and Michael Massey for assistance with XAS data collection. This research was funded by the U.S. Department of Energy (DOE), Office of Science, Office of Biological and Environmental Research under contracts DE-FG02-07ER-6436 (Montana State University) and DE-AC02-05CH11231 (Lawrence Berkeley National Laboratory; operated by the University of California) and is partially based upon work supported through the Lawrence Berkeley National Laboratory's Sustainable Systems Scientific Focus Area.

References

This article references 39 other publications.

1. (a) (GAO), U. S. G. A. O., Nuclear Waste Problems Associated with DOE's Inactive Waste Sites, GAO/RCED-88–169 **1988a**;

(b) (GAO)., U. S. G. A. O. *Nuclear Waste*, *Supplemental Information on Problems at DOE's Inactive Waste Sites*; U.S. Government Accounting Office: Washington, DC, **1988b**; pp GAO/RCED-88–229FS.

2. Smythe, C.; Bierley, D.; Bradshaw, M. US regulatory framework for long-term management of uranium mill tailings *Journal of the Mine Ventilation Society of South Africa* **1995**, 48 (10) 246– 253

3. Abdelouas, A.; Lutze, W.; Nuttall, E. Chemical reactions of uranium in ground water at a mill tailings site *J. Contam. Hydrol.* **1998**, 34 (4) 343– 361 DOI: 10.1016/S0169-7722(98)00097-7

[Crossref], [CAS]

4. Processing Sites and Disposal Site; U.S. Department of Energy: Rifle, CO, **2013**.

5. Thompson, A.; Chadwick, O. A.; Rancourt, D. G.; Chorover, J. Iron-oxide crystallinity increases during soil redox oscillations *Geochim. Cosmochim. Acta* **2006**, 70 (7) 1710– 1727 DOI: 10.1016/j.gca.2005.12.005

[Crossref], [CAS]

6. Rancourt, D. G.; Thibault, P. J.; Mavrocordatos, D.; Lamarche, G. Hydrous ferric oxide precipitation in the presence of nonmetabolizing bacteria: Constraints on the mechanism of a biotic effect *Geochim. Cosmochim. Acta* **2005**, 69 (3) 553– 577 DOI: 10.1016/j.gca.2004.07.018

[Crossref], [CAS]

7. Liang, L. Y.; McCarthy, J. F.; Jolley, L. W.; McNabb, J. A.; Mehlhorn, T. L. Iron dynamics - transformation of Fe(II)/Fe(III) during injection of natural organic-matter in a sandy aquifer *Geochim. Cosmochim. Acta* **1993**,57 (9) 1987– 1999 DOI: 10.1016/0016-7037(93)90088-E

[Crossref], [CAS]

8. Pullin, M. J.; Cabaniss, S. E. The effects of pH, ionic strength, and iron-fulvic acid interactions on the kinetics of nonphotochemical iron transformations. I. Iron(II) oxidation and iron(III) colloid formation *Geochim. Cosmochim. Acta* **2003**, 67 (21) 4067– 4077 DOI: 10.1016/S0016-7037(03)00366-1

[Crossref], [CAS]

9. Brown, Jr., G. E.; Trainor, T. P.; Chaka, A. M., Geochemistry of mineral surfaces and factors affecting their chemical reactivity. In *Chemical Bonding at Surfaces and Interfaces*; Nilsson, A.; Patterson, L. G. M.;Norskov, J., Ed.; Elsevier: New York, **2007**; pp 457– 509.

10. Read, D. Geochemical Modeling of Uranium Redistribution in the Osamu Utsumi Mine, Pocos-De-Caldas *J. Geochem. Explor.* **1992**, 45 (1–3) 503– 520 DOI: 10.1016/0375-6742(92)90137-W

[Crossref], [CAS]

11. Stubbs, J. E.; Elbert, D. C.; Veblen, D. R.; Zhu, C. Electron microbeam investigation of uranium-contaminated soils from Oak Ridge, TN, USA *Environ. Sci. Technol.* **2006**, 40 (7) 2108– 2113 DOI: 10.1021/es0518676

[ACS Full Text], [CAS]

12. Campbell, K. M.; Kukkadapu, R. K.; Qafoku, N. P.; Peacock, A. D.; Lesher, E.; Williams, K. H.; Bargar, J. R.;Wilkins, M. J.; Figueroa, L.; Ranville, J.; Davis, J. A.; Long, P. E. Geochemical, mineralogical and microbiological characteristics of sediment from a naturally reduced zone in a uranium-contaminated aquifer *Appl. Geochem.* **2012**, 27 (8) 1499– 1511 DOI: 10.1016/j.apgeochem.2012.04.013

[Crossref], [CAS]

13. (a) Gomez, P.; Garralon, A.; Buil, B.; Turrero, M. J.; Sanchez, L.; de la Cruz, B. Modeling of geochemical processes related to uranium mobilization in the groundwater of a uranium mine *Sci. Total Environ.* **2006**,366 (1) 295– 309 DOI: 10.1016/j.scitotenv.2005.06.024

[Crossref], [PubMed], [CAS]

(b) Reed, D. T.;Pepper, S. E.; Richmann, M. K.; Smith, G.; Deo, R.; Rittmann, B. E. Subsurface bio-mediated reduction of higher-valent uranium and plutonium *J. Alloys Compd.* **2007**, 444–445, 376– 82 DOI: 10.1016/j.jallcom.2007.06.015

[Crossref], [CAS]

14. (a) Murakami, T.; Ohnuki, T.; Isobe, H.; Sato, T. Mobility of uranium during weathering *Am. Mineral.* **1997**, 82(9–10) 888– 899

[Crossref], [CAS]

(b) Gu, B. H.; Brooks, S. C.; Roh, Y.; Jardine, P. M. Geochemical reactions and dynamics during titration of a contaminated groundwater with high uranium, aluminum, and calcium*Geochim. Cosmochim. Acta* **2003**, 67 (15) 2749– 2761 DOI: 10.1016/S0016-7037(03)00097-8

[Crossref], [CAS]

(c) Payne, T. E.; Airey, P. L. Radionuclide migration at the Koongarra uranium deposit, Northern Australia - Lessons from the Alligator Rivers analogue project *Physics and Chemistry of the Earth* **2006**, 31(10–14) 572– 586 DOI: 10.1016/j.pce.2006.04.008

[Crossref]

15. (a) Duff, M. C.; Coughlin, J. U.; Hunter, D. B. Uranium co-precipitation with iron oxide minerals *Geochim. Cosmochim. Acta* **2002**, 66 (20) 3533– 3547 DOI: 10.1016/S0016-7037(02)00953-5

[Crossref], [CAS]

(b)Nico, P. S.; Stewart, B. D.; Fendorf, S. Incorporation of Oxidized Uranium into Fe (Hydr)oxides during Fe(II) Catalyzed Remineralization *Environ. Sci. Technol.* **2009**, 43 (19) 7391– 7396 DOI: 10.1021/es900515q

[ACS Full Text], [CAS]

(c) Boland, D. D.; Collins, R. N.; Payne, T. E.; Waite, T. D. Effect of Amorphous Fe(III) Oxide Transformation on the Fe(II)-Mediated Reduction of U(VI) *Environ. Sci. Technol.* **2011**, 45 (4)1327– 1333 DOI: 10.1021/es101848a

[ACS Full Text], [CAS]

(d) Boland, D. B.; Collins, R. N.;Glover, C. J.; Payne, T. E.; Waite, D. T. Reduction of U(VI) by Fe(II) during the Fe(II)-accelerated transformation of ferrihydrite *Environ. Sci. Technol.* **2014**, 48 (16) 9086– 9093 DOI: 10.1021/es501750z

[ACS Full Text], [CAS]

16. Wagai, R.; Mayer, L. M. Sorptive stabilization of organic matter in soils by hydrous iron oxides *Geochim. Cosmochim. Acta* **2007**, 71 (1) 25– 35 DOI: 10.1016/j.gca.2006.08.047

[Crossref], [CAS]

17. Chao, T. T.; Zhou, L. Extraction techniques for selective dissolution of amorphous iron-oxides from soils and sediments *Soil Science Society of America Journal* **1983**, 47 (2) 225– 232 DOI: 10.2136/sssaj1983.03615995004700020010x

[Crossref], [CAS]

18. Brooks, S. C.; Taylor, D. L.; Jardine, P. M. Reactive transport of EDTA-complexed cobalt in the presence of ferrihydrite *Geochim. Cosmochim. Acta* **1996**, 60 (11) 1899– 1908 DOI: 10.1016/0016-7037(96)00064-6

[Crossref], [CAS]

19. Hammersley, A. P. *Fit2D V9.129 Reference Manual V. 3.1; ESFR Internal Report ESRF98HA01*; T. European Synchrotron Radiation Facility: Grenoble, France, **1998**; p 306.

20. Webb, S. M. SIXPack: a graphical user interface for XAS analysis using IFEFFIT *Phys. Scr.* **2005**, 2005(T115) 4 DOI: 10.1238/Physica.Topical.115a01011

[Crossref]

21. Zachara, J. M.; Long, P. E.; Bargar, J. R.; Davis, J. A.; Fox, P.; Fredrickson, J. K.; Freshley, M. D.;Konopka, A.; Lui, C.; McKinley, J. P.; Rockhold, M.; Williams, K. H.; Yabusaki, S. B. Persistence of uranium groundwater plumes: Contrasting mechanisms at two DOE sites in the groundwater-river interaction zone *J. Contam. Hydrol.* **2013**, 147, 45– 72 DOI: 10.1016/j.jconhyd.2013.02.001

[Crossref], [PubMed], [CAS]

22. (a) De Endredy, A. S. Estimation of free iron oxides in soils and clays by a photolytic method *Clay Miner.***1963**, 5, 209– 217 DOI: 10.1180/claymin.1963.005.29.07

[Crossref], [CAS]

(b) Jambor, J. L.; Dutrizac, J. E.Occurrence and constitution of natural and synthetic ferrihydrite, a widespread iron oxyhydroxide *Chem. Rev.* **1998**, 98 (7) 2549– 2585 DOI: 10.1021/cr970105t

[ACS Full Text], [CAS]

23. (a) Carlson, L.; Bigham, J. M.; Schwertmann, U.; Kyek, A.; Wagner, F. Scavenging of As from acid mine drainage by schwertmannite and ferrihydrite: a comparison with synthetic analogues *Environ. Sci. Technol.***2002**, 36 (8) 1712– 1719 DOI: 10.1021/es0110271

[ACS Full Text], [CAS]

(b) Kumpulainen, S.;Carlson, L.; Raisanen, M.-L. Seasonl variations of ochreous precipitates in mine effluents in Finland *Appl. Geochem.* **2007**, 22 (4) 760– 777 DOI: 10.1016/j.apgeochem.2006.12.016

[Crossref], [CAS]

24. Cismasu, A. C.; Williams, K. H.; Nico, P. S., Selective degradation of mineral-bound organic matter under fluctuating redox conditions Environ. Sci. Technol. in review.

[PubMed]

25. (a) Kleber, M.; Mikutta, R.; Torn, M. S.; Jahn, R. Poorly crystalline mineral phases protect organic matter in acid subsoil horizons *Eur. J. Soil Sci.* **2005**, 56 (6) 717– 725 DOI: 10.1111/j.1365-2389.2005.00706.x

[Crossref], [CAS]

(b) Thompson, A.; Rancourt, D. G.; Chadwick, O. A.; Chorover, J. Iron solid-phase differentiation along a redox gradient in basaltic soils *Geochim. Cosmochim. Acta* **2011**, 75 (1) 119– 133DOI: 10.1016/j.gca.2010.10.005

[Crossref]

26. Fortin, D.; Leppard, G. G.; Tessier, A. Characteristics of lacustrine diagenetic iron oxyhydroxides *Geochim. Cosmochim. Acta* **1993**, 57 (18) 4391– 4404 DOI: 10.1016/0016-7037(93)90490-N

[Crossref], [CAS]

27. .Lalonde, K.; Mucci, A.; Ouellet, A.; Gelinas, Y., Preservation of organic matter in sediments promoted by iron. *Nature* **2012**, 483 (7388), 198– 200. DOI: 10.1038/nature10855

[Crossref], [PubMed], [CAS]

28. (a) Hansel, C. M.; Learman, D. R.; Lentini, C. J.; Ekstrom, E. B. Effect of adsorbed and substituted Al on Fe(II)-induced mineralization pathways of ferrihydrite *Geochim. Cosmochim. Acta* **2011**, 75 (16) 4653– 4666DOI: 10.1016/j.gca.2011.05.033

[Crossref], [CAS]

(b) Ekstrom, E. B.; Learman, D. R.; Madden, A. S.;Hansel, C. M. Contrasting effects of Al substitution on microbial reduction of Fe(III) (hydr)oxides *Geochim. Cosmochim. Acta* **2010**, 74 (24) 7086– 7099 DOI: 10.1016/j.gca.2010.09.008

[Crossref], [CAS]

(c)Masue-Slowey, Y.; Loeppert, R. H.; Fendorf, S. Alteration of ferrihydrite reductive dissolution and transformation by adsorbed As and structural Al: Implications for As retention *Geochim. Cosmochim. Acta***2011**, 75 (3) 870– 886 DOI: 10.1016/j.gca.2010.11.016

[Crossref], [CAS]

29. Borch, T.; Masue, Y.; Kukkadapu, R. K.; Fendorf, S. Phosphate imposed limitations on biological reduction and alteration of ferrihydrite *Environ. Sci. Technol.* **2007**, 41 (1) 166– 172 DOI: 10.1021/es060695p

[ACS Full Text], [CAS]

30. Jones, A. M.; Collins, R. N.; Rose, J.; Waite, T. D. The effect of silica and natural organic matter on the Fe(II)-catalysed transformation and reactivity of Fe(III) minerals *Geochim. Cosmochim. Acta* **2009**, 73 (15)4409– 4422 DOI: 10.1016/j.gca.2009.04.025

[Crossref], [CAS]

31. (a) Henneberry, Y. K.; Kraus, T. E. C.; Nico, P. S.; Horwath, W. R., Structural stability of coprecipitated natural organic matter and ferric iron under reducing conditions. *Org. Geochem.* **2012**, 48, 81– 89 DOI: 10.1016/j.orggeochem.2012.04.005 .

[Crossref], [CAS]

(b) Shimizu, M.; Zhou, J. H.; Schroder, C.; Obst, M.;Kappler, A.; Borch, T., Dissimilatory Reduction and Transformation of Ferrihydrite-Humic Acid Coprecipitates. *Environ. Sci. Technol.* **2013**, 47 (23), 13375– 13384 DOI: 10.1021/es402812j .

[ACS Full Text], [CAS]

32. Wilke, M.; Farges, F.; Petit, P. E.; Brown, G. E.; Martin, F. Oxidation state and coordination of Fe in minerals: An FeK-XANES spectroscopic study *Am. Mineral.* **2001**, 86 (5–6) 714– 730

[Crossref], [CAS]

33. Takahashi, Y.; Higashi, M.; Furukawa, T.; Mitsunobu, S. Change of iron species and iron solubility in Asian dust during the long-range transport from western China to Japan *Atmos. Chem. Phys.* **2011**, 11 (21)11237– 11252 DOI: 10.5194/acp-11-11237-2011

[Crossref], [CAS]

34. (a) Cismasu, A. C.; Levard, C.; Michel, F. M.; Brown, G. E., Properties of impurity-bearing ferrihydrite II: Insights into the surface structure and composition of pure, Al- and Si-bearing ferrihydrite from Zn(II) sorption experiments and Zn K-edge X-ray absorption spectroscopy. *Geochim. Cosmochim. Acta* **2013**, 119,46– 60 DOI: 10.1016/j.gca.2013.05.040 .

[Crossref], [CAS]

(b) Dyer, L. G.; Chapman, K. W.; English, P.;Saunders, M.; Richmond, W. R., Insights into the crystal and aggregate structure of Fe3+ oxide/silica co-precipitates. *Am. Mineral.* **2012**, 97 (1), 63– 69 DOI: 10.2138/am.2011.3874 .

[Crossref], [CAS]

35. Yang, Y.; Saiers, J. E.; Barnett, M. O. Impact of Interactions between Natural Organic Matter and Metal Oxides on the Desorption Kinetics of Uranium from Heterogeneous Colloidal Suspensions *Environ. Sci. Technol.* **2013**, 47 (6) 2661– 2669 DOI: 10.1021/es304013r

[ACS Full Text], [CAS]

36. Stewart, B. D.; Nico, P. S.; Fendorf, S. Stability of Uranium Incorporated into Fe (Hydr)oxides under Fluctuating Redox Conditions *Environ. Sci. Technol.* **2009**, 43 (13) 4922– 4927 DOI: 10.1021/es803317w

[ACS Full Text], [CAS]

37. (a) Wu, W.-M.; Carley, J.; Luo, J.; Ginder-Vogel, M. A.; Cardenas, E.; Leigh, M. B.; Hwang, C.; Kelly, S. D.;Ruan, C.; Wu, L.; Van Nostrand, J.; Gentry, T.; Lowe, K.; Mehlhorn, T.; Carroll, S.; Luo, W.; Fields, M. W.;Gu, B.; Watson, D.; Kemner, K. M.; Marsh, T.; Tiedje, J.; Zhou, J.; Fendorf, S.; Kitanidis, P. K.;Jardine, P. M.; Criddle, C. S. In situ bioreduction of uranium (VI) to submicromolar levels and reoxidation by dissolved oxygen *Environ. Sci. Technol.* **2007**, 41 (16) 5716– 5723 DOI: 10.1021/es062657b

[ACS Full Text], [CAS]

(b) Singer, D. M.; Zachara, J. M.; Brown, G. E., Jr. Uranium Speciation As a Function of Depth in Contaminated Hanford Sediments - A Micro-XRF, Micro-XRD, and Micro- And Bulk-XAFS Study *Environ. Sci. Technol.* **2009**, 43 (3) 630– 636 DOI: 10.1021/es8021045

[ACS Full Text], [CAS]

38. Manceau, A.; Marcus, M. A.; Tamura, N., Quantitative speciation of heavy metals in soils and sediments by synchrotron X-ray techniques. In *Applications of 623 Synchrotron Radiation in Low-Temperature Geochemistry and Environmental 624 Sciences*; Fenter, P. A.; Rivers, M. L.; Sturchio, N. C.; Sutton, S. R., Eds.; **2002**; Vol. 49, pp 341– 428.

[Crossref]

39. (a) Hansel, C. M.; Fendorf, S.; Sutton, S.; Newville, M. Characterization of Fe plaque and associated metals on the roots of mine-waste impacted aquatic plants *Environ. Sci. Technol.* **2001**, 35 (19) 3863– 3868 DOI: 10.1021/es0105459

[ACS Full Text], [CAS]

(b) Cornell, R. M.; Schwertmann, U. *The Iron Oxides: Structure, Properties, Reactions, Occurences and Uses*; Wiley-VCH, **2003**.

[Crossref]